Foreshock activity related to enhanced aftershock production

D. Marsan, A. Helmstetter, M. Bouchon, Pierre Dublanchet

AGU PUBLICATIONS

Geophysical Research Letters

RESEARCH LETTER
10.1002/2014GL061219

Key Points:
- Foreshocks lead to enhanced aftershock production
- Aseismic slip before and after the main shock is a likely cause

Supporting Information:
- Readme
- Figures S1–S9 and Tables S1 and S2

Correspondence to:
D. Marsan,
david.marsan@univ-savoie.fr

Citation:
Marsan, D., A. Helmstetter, M. Bouchon, and P. Dublanchet (2014), Foreshock activity related to enhanced aftershock production, *Geophys. Res. Lett.*, *41*, 6652–6658, doi:10.1002/2014GL061219.

Received 14 JUL 2014
Accepted 4 SEP 2014
Accepted article online 6 SEP 2014
Published online 7 OCT 2014

Foreshock activity related to enhanced aftershock production

D. Marsan[1], A. Helmstetter[2], M. Bouchon[2], and P. Dublanchet[3,4]

[1]ISTerre, Université de Savoie, CNRS, Le Bourget du Lac, France, [2]ISTerre, CNRS, Université Joseph Fourier, Grenoble, France, [3]Institut de Physique du Globe de Paris, Paris, France, [4]Schweizerischer Erdbebendienst, ETH, Zürich, Switzerland

Abstract Foreshock activity sometimes precedes the occurrence of large earthquakes, but the nature of this seismicity is still debated, and whether it marks transient deformation and/or slip nucleation is still unclear. We here study at the worldwide scale how foreshock occurrence affects the postseismic phase and find a significant positive correlation between foreshock and aftershock activities: earthquakes preceded by accelerating seismicity rates produce 40% more aftershocks on average, and the length of the aftershock zone after 20 days is 20% larger. These observations cannot be reproduced by standard earthquake clustering models that predict the accelerating pattern of foreshock occurrence but not its impact on aftershock activity. This strongly suggests that slow deformation transients, possibly related to episodic creep, could initiate prior to the main shock and extend past the coseismic phase, resulting in compound ruptures that include a very long period (up to tens of days) component.

1. Introduction

Foreshocks are frequently, although not always, detected prior to large shocks. Numerous studies have addressed the possible existence of a causal effect between these foreshocks and the subsequent main shock, leading to contrasting conclusions (see *Mignan* [2014] for a recent review). It has been argued that episodes of aseismic deformation could sometimes precede the main shock; clear instances of such episodes, possibly linked to fault creep, are to be found in subduction zones [*Kato et al.*, 2012] and on continental strike-slip faults [*Bouchon et al.*, 2011]. In both cases, repeating ruptures of one or several fault patches over short time scales (minutes to days) effectively suggest rapid loading of the asperities, incompatible with low, secular tectonic deformation rates. What causes these sudden creep events at seismogenic depths still remains unknown.

The transient uncoupling of the fault undergoing foreshock activity does not necessarily stop with the main rupture and could continue during the postseismic phase. This creep would then add to the "normal" afterslip typically following any main shock. As a result, aftershock sequences could be affected by the initial deformation transient. Since aftershocks are abundant and ubiquitous, they represent a privileged phenomena that potentially bears the signature of an initial uncoupling of the fault.

2. Data and Methods

We analyze the worldwide composite earthquake catalog provided by the Advanced National Seismic System (ANSS) (quake.geo.berkeley.edu/anss), from 1 January 1980 to 19 September 2013. Only $m \geq 4.0$ earthquakes are considered; the influence of this cutoff magnitude on the results is investigated in the supporting information, section "Influence of the cut-off magnitude." We select as main shocks all $m \geq 6.5$ earthquakes occurring after 1 January 1981 that are not preceded in the last year by $m \geq 6.0$ earthquakes within an epicentral distance of $10 \times L(m) = 0.05 \times 10^{0.5m}$ (in km), where m is the magnitude of the first shock and L is its rupture radius (half its rupture length). This selection criterion is intended to remove from the list of main shocks those which precursory activity could be contaminated by aftershock sequences of preceding large shocks. This leaves us with 612 main shocks.

We measure possible precursory seismicity acceleration before and within 50 km (in epicentral distance) of each main shock, by running the algorithm of *Bouchon et al.* [2013] that computes the probability p that the observed acceleration could be due to chance, i.e., to natural fluctuations in the dynamics of seismicity: we consider the time series of earthquake occurrence times relative to the main shock $t_1, t_2, \ldots < 0$, within 50 km of the main shock epicenter. Then, for a fixed duration T, we compute the acceleration index n as follows:

1. We start with $n = 0$.

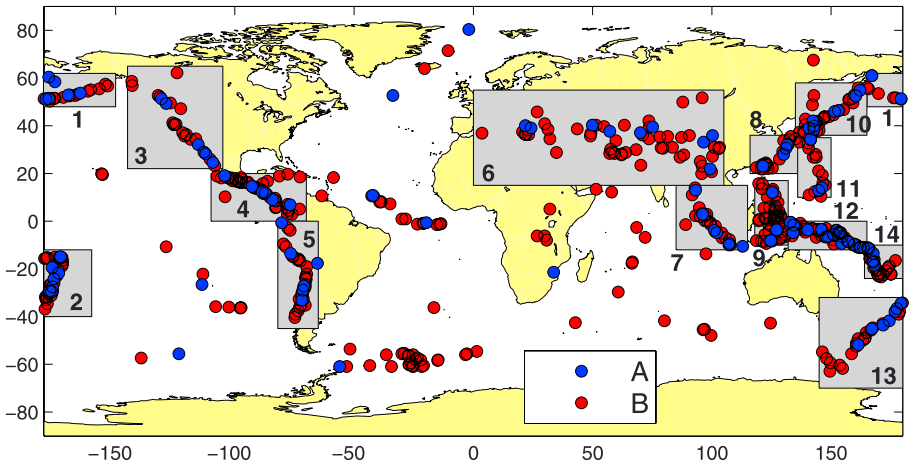

Figure 1. Location of the 612 selected main shocks. Blue: main shocks of population A, characterized by acceleration of the earthquake activity prior to the main shock. Red: main shocks of population B, with no acceleration. The grey boxes and indexes refer to the zones studied in the supporting information, section "Dependence on location."

2. We divide the time interval $-T < t < 0$ into two: $-T < t < -T/2$ (N_1 events) and $-T/2 < t < 0$ (N_2 events). If there is an acceleration, then $N_2 > N_1$. So either (i) $N_1 \geq N_2$, in which case we stop and keep the current value of n, or (ii) $N_1 < N_2$, then $n = n + 1$, $T = T/2$ (we now analyze the time interval $T/2 < t < 0$), and start again at stage (2). We thus obtain an index n relative to the initial duration T. We apply this treatment with eight initial values of T: 1 day, 5 days, 10 days, 1 month, 2 months, 3 months, 6 months, and 1 year. We thus have eight values of n and keep the largest. We finally compare this maximum value of n with Monte Carlo simulations of stationary time series. We generate 10^3 Poisson time series with the rate equal to the sampling rate of the real time series (over 1 year). For each, we compute the largest n. We then count the number of times this index is equal or larger than the real n and thus end up with the probability p that the real n or better can be obtained by a random process. This probability p is thus the probability that the observed acceleration can be obtained by chance.

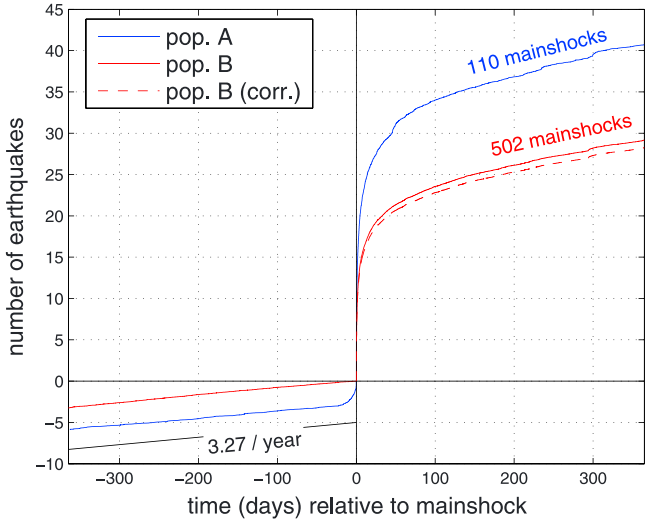

Figure 2. Stacked number of $m \geq 4$ earthquakes within 50 km of the main shock epicenter, for the two populations A ($p \leq 0.1$) and B ($p > 0.1$), divided by the number of sequences (110 and 502, respectively). The mean rate prior to the main shocks of population B is 3.27 per year, while it is 3.04 per year for those of population A (for $t < -50$ days to avoid the acceleration phase); the difference is not statistically significant (at 16.1%). Red dashed line: aftershocks of population B after correcting for the difference in magnitude distribution for the two populations (see text).

3. Relationship Between Foreshock and Aftershock Activities

We divide the main shocks into two populations: (A) those with $p \leq 0.1$, hence characterized by significant acceleration, and (B) the others. We count 110 main shocks in A and 502 main shocks in B. The repartition of these two populations does not exhibit any obvious geographic pattern (Figure 1). We investigate in Figure 2 how this precursory activity affects aftershock sequences, by computing the stacked number of earthquakes within 50 km, starting 1 year before the main shock and finishing 1 year after, for both populations. While population B main shocks are preceded by a

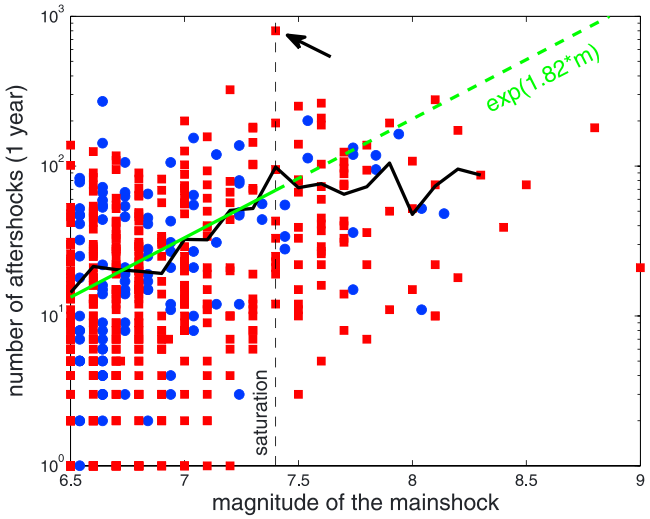

Figure 3. Number of aftershocks (for 1 year and within 50 km) function of the main shock magnitude, for the two populations (A: blue and B: red). The blue dots have been slightly shifted to the right for clarity. The numbers averaged for magnitude bins of length 0.1 give the black curve. The number of aftershocks saturates at $m = 7.4$, as the rupture radius becomes comparable to 50 km (dashed line). Green: fit to the average number of aftershocks (black curve) up to the saturation at $m = 7.4$. The arrow points to the *M*7.4, 21 December 2010 Bonin earthquake, which is characterized by a remarkably strong aftershock sequence.

constant rate of activity, those of population A occur after a late phase of accelerating activity which starts about 20 days prior to the main shock.

Remarkably, the average number of aftershocks N per sequence is greater if acceleration was present before the main shock (population A): we find $N_A = 40.7$ for population A sequences and $N_B = 29.1$ for population B, for 1 year after the main shock, hence a 40% increase from N_B. This correlation between precursory acceleration and the number of aftershocks is significant, as other intervals of p used to define population A (i.e., other than $0 \le p \le 0.1$ used here) lead to weaker or no relationship at all, see supporting information, section "Significance of the correlation between precursory acceleration and the number of aftershocks." This feature is also present at regional scale for most active regions, with the notable exception of North America (see supporting information, section "Dependence on location") due to a mixing of oceanic transform fault main shocks with continental main shocks in this region.

Five simple mechanisms can be thought of to explain this correlation: (1) main shocks in population A tend to have greater magnitudes than those of population B, hence triggering more productive aftershock sequences; (2) the main shocks in A occur in places where the long-term averaged seismicity rate is higher than normal, so that the number of aftershocks is greater, as predicted by friction models of earthquake triggering [*Dieterich*, 1994]; (3) the preshocks that cause the acceleration trigger their own aftershocks, which add to those of the main shock, resulting in a greater number of aftershocks overall; (4) the aftershocks of population A tend to be bigger than those of population B, thus triggering more of their own aftershocks; and (5) magnitude completeness is different for populations A and B.

Mechanism (1) is simply refuted by observing that the mean magnitude $m_A = 6.88$ of main shocks in population A is less than $m_B = 6.90$ for population B. We use a productivity law for which the number N of aftershocks within 50 km triggered by a magnitude m main shock depends on m as $\exp(\alpha\, m)$, saturating at large m when the aftershock zone has a radius greater than 50 km; fitting this law to the data gives $\alpha = 1.82$ and a saturation magnitude of 7.4 (see Figure 3). Using these values, we obtain $N_B/N_A = 1.03$. Correcting for this bias in favor of N_B gives the dashed line of Figure 2, further enhancing the difference between the two populations.

The spatial distribution of main shocks does not show a clear tendency of population A main shocks to cluster in specific regions that are more seismically active than the rest (Figure 1). Moreover, the increase in aftershock productivity for population A main shocks is found to be largely independent of the tectonic region (see supporting information, section "Dependence on location"). Finally, we note that the preseismic rate within 50 km of the main shock is the same for the two populations, apart from the sudden acceleration characteristic of population A (Figure 2). All these observations argue against mechanism (2).

Mechanism (3) can be investigated by considering that every preshock triggers aftershocks with rate $K(m)/(t+c)$ in the 50 km radius region surrounding the main shock, with $K(m) = k \exp(1.82 \times m)$ if $m \le 7.4$ and $K(m) = k \exp(1.82 \times 7.4)$ if $m > 7.4$ (saturation). We find that the average K of $K(m)$ over the 612 main shocks

equals 3.6, yielding $k = 8.20 \times 10^{-6}$ (see Figure S9). Up to 1 year after the main shock, the expected number of aftershocks in population A attributable to preshocks occurring in the year before the main shock is

$$N_A' = \frac{1}{110}\sum_n K(m_n)[\log(365 + c - t_n) - \log(c - t_n)] \quad (1)$$

where the summation is done on all preshocks (index n) of magnitude m_n occurring at time -365 days $< t_n < 0$ before the main shock. Computing N_B' the same way, we find that $N_A' - N_B' = 1.20$, thus accounting for only 10.3% of the total difference $N_A - N_B = 11.6$. A tenfold (9.55 precisely) increase of the productivity parameter k would be needed during the last 20 days of population A sequences, prior to the main shock, for these foreshocks to explain the +11.6 gain in aftershock number.

Mechanism (4) seems plausible after observing that the mean productivity K of population A aftershocks is 54% greater than for population B aftershocks, due to a difference in their magnitudes. In effect, both aftershock populations are characterized by indistinguishable Gutenberg-Richter laws with $b = 1.21 \pm 0.06$ (population A) and $b = 1.18 \pm 0.03$ (population B) (see Figure S1). However, one of the main shocks in population A is the M_w7.5 foreshocks of the 2011 M_w9.1 Tohoku earthquake and thus has the latter as one of its "aftershock." Removing the sequence with this M_w7.5 main shock from our analysis leads to an increase of K of only 8% rather than 54% but does not suppress the observed correlation: the gain in aftershock production for population A sequences is then 34% rather than 40%. Moreover, the Tohoku sequence, with the M_w7.5 foreshock occurring at the end of a 2 month long foreshock swarm [*Ando and Imanishi*, 2011; *Kato et al.*, 2012], is an important example of how foreshock activity and enhanced aftershock production can be linked and as such should be fully considered rather than removed from the statistics.

Magnitude completeness is the same for the aftershocks of populations A and B (see Figure S1), and it therefore does not affect the difference in the number of observed aftershocks. We moreover show in the supporting information, section "Influence of cut-off magnitude," that the correlation also exists when using $m_c = 5.0$ instead of 4.0.

4. Comparison With Clustering Models

The observed relationship between foreshock and aftershock activities cannot be explained by standard earthquake clustering models. We here consider the epidemic type aftershock sequence (ETAS) model [*Ogata*, 1988] as a null hypothesis, according to which acceleration prior to the main shock is only a consequence of earthquake clustering properties [*Helmstetter and Sornette*, 2003; *Hardebeck et al.*, 2008]. This model effectively predicts acceleration on ensemble average, prior to any earthquake unconditioned on its magnitude (i.e., the averaged acceleration is the same for all earthquakes regardless of their magnitudes). It, however, does not predict the observed correlation between acceleration and aftershock production, as we now demonstrate.

We run simulations using an ETAS model with triggering rate density $\lambda(x, y, t) = \mu + \sum \lambda_i(x, y, t)$ where μ is the background rate density, the sum being performed on all earthquakes i that occur before time t, and λ_i being the rate density of triggering due to earthquake i. We take $\lambda_i(x, y, t) = A_i e^{\alpha m_i}(t - t_i + 0.08)^{-1} \times \frac{(\gamma-1)L_i^{\gamma-1}}{2\pi\left(r^2+L_i^2\right)^{(\gamma+1)/2}}$, in agreement with the results of Figure S9. The distance r is between earthquake i and the position (x, y), and $L_i = L_0 \times 10^{0.5m_i}$ (in km) is the rupture length of earthquake i. To avoid run away sequences, as the number of aftershocks grows to infinity for any main shock with this choice of triggering kernel, we limit triggering to the first 10 years after any main shock. The earthquakes occupy a 2000 km × 2000 km square with periodic boundaries, and the background rate over this area is three earthquakes per day, with background earthquakes occurring according to a uniform spatial distribution over the square. Magnitudes are drawn randomly from the sample distribution of the ANSS catalog with $m \geq 4$. In order to reproduce the distribution of the number of aftershocks per main shock of Figure 3, we fix $\alpha = 2.3$, $L_0 = 0.008$ km, and $\gamma = 3.5$. The choice of α is done so to use the largest acceptable value ($\alpha < b \ln 10$) for this model; large α values enhance the average acceleration seen before main shocks when stacking over sequences. Moreover, the dispersion of the data points in Figure 3 requires that A_i is variable from one earthquake to the other. We find that taking $A_i = 3 \times 10^{-7}(1.8u + 0.1)$, where $0 < u < 1$ is a uniform law, generates a realistic variability.

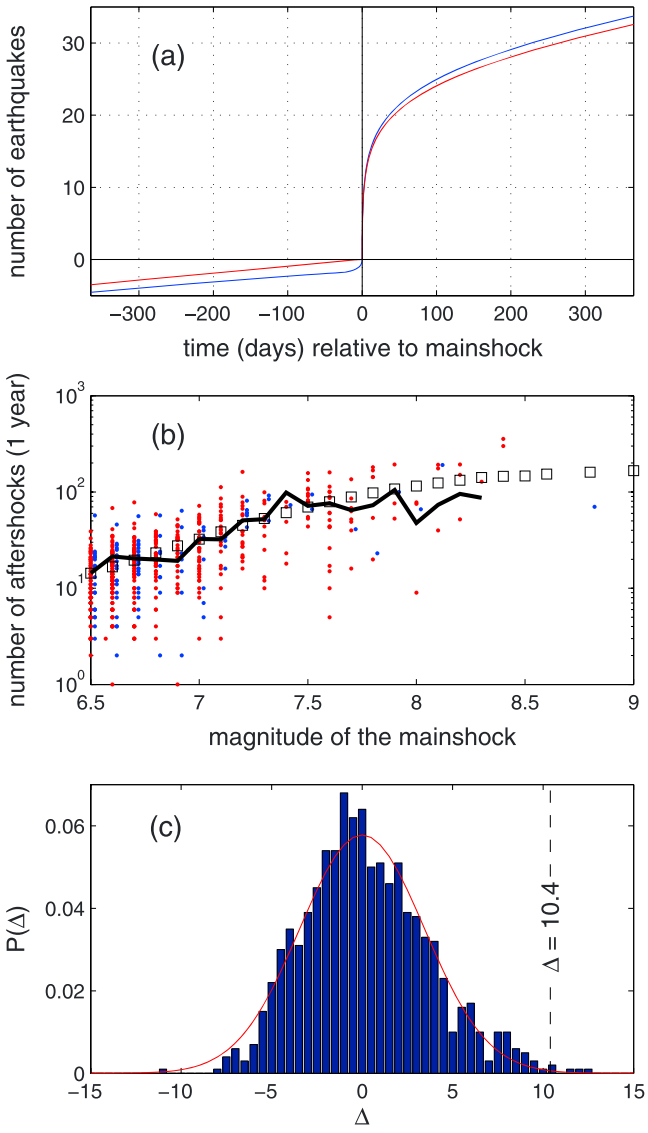

Figure 4. Comparison with synthetic ETAS earthquake catalogs. (a) Same as Figure 2; extra aftershocks in population A are here, by construction, aftershocks of the foreshocks. (b) Same as Figure 3; the blue and red dots are for a random subset of 110 and 502 synthetic sequences of populations A and B main shocks. Black squares are numbers averaged over the 1000 synthetics (95,951 and 588,619 sequences in total for populations A and B, respectively). The average numbers for the real data are shown with the black curve for comparison. (c) Distribution of Δ, the difference between populations A and B in the numbers of aftershocks triggered in 1 year, corrected for aftershocks triggered by foreshocks according to equation (1). The best centered Gaussian fit is displayed in red. The observed Δ value of 10.4 for the real data is shown for reference.

We draw 1000 synthetic catalogs, each catalog having a duration of 50,000 years. We obtain on average 95.9 main shocks in population A and 588.6 in population B, for each catalog. We compute the mean numbers N_A and N_B of aftershocks per sequence and correct N_B for differences in the magnitude distribution of the main shocks. We subtract from $N_A - N_B$ the difference $N_A' - N_B'$ of aftershocks triggered by foreshocks, taking the exact same relation (equation (1)) as with the real data. We plot the distribution of $\Delta = N_A - N_B - (N_A' - N_B')$ in Figure 4c. A difference greater than $\Delta = 10.4$ as found with the real data is only observed to occur 5 times for our 1000 synthetics. The probability of $\Delta > 10.4$ as given by the Gaussian fits of Figure 4c is 0.13%. This shows that natural fluctuations in the ETAS model are very unlikely to explain the statistically increased triggering of population A main shocks. Moreover, the probability that such natural fluctuations cause nine out of 14 tectonic regions to unambiguously display this feature is very low if earthquake clustering properties of the ETAS model were the only reason for increased triggered. Inward migration of foreshocks, as predicted by ETAS models [*Helmstetter and Sornette*, 2003], is observed for population A foreshocks, although not as strongly as with our synthetic catalogs.

5. Spreading of Aftershock Zone

The observed correlation thus cannot be explained by normal earthquake activity characterized by ensemble-averaged clustering laws only, although the latter account for some limited contribution to this observation, nor by observational biases, hinting toward an aseismic process not obeying these laws. We moreover observe that aftershocks of population A sequences are more spread in space than those of population B sequences (Figure 5). This difference in spatial distribution is well accounted for if the rupture length of population A main shocks is modeled as being 20% larger than what it should normally be (i.e., than the rupture length of population B main shocks of similar magnitude) after 20 days. Synthetic ETAS catalogs using the same parameterization as above exhibit a spreading as well, but limited to only 5% rather than 20%. This increase in L depends on the analyzed time interval after the main shock, decaying from 25% after only 1 day to 11% after 1 year, the latter time interval being then contaminated

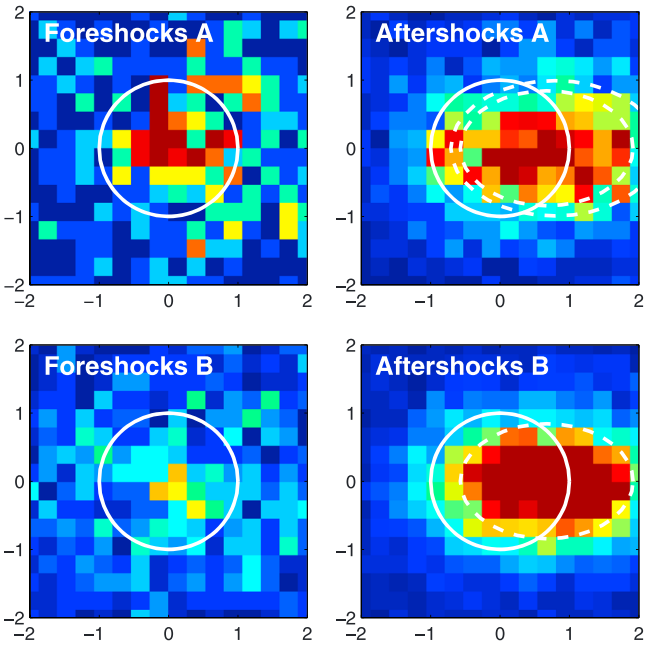

Figure 5. Spatial distributions of 1 year of foreshocks and 20 days of aftershocks, for the two populations. Epicentral distances to the main shock have been normalized by the rupture radius $L = 0.005 \times 10^{0.5m}$ (in km), and horizontally rotated for each sequence so that the $y = 0$ line is the direction best cutting the 1 year aftershock distribution, and oriented so that more than 50% of the aftershocks lie at $x > 0$. All graphs have the same color coding. The unit circles are shown, together with the 1 s confidence ellipse for the aftershocks (dashed lines). On the upper right graph, the smaller confidence ellipse of the aftershocks of population B is superposed to the larger one for population A to demonstrate the ×1.20 spreading of the latter.

by background earthquakes. Assuming a $e^{1.82 \times m} = L(m)^{2 \times 1.82/\log(10)} = L(m)^{1.58}$ scaling of aftershock productivity with main shock magnitude and/or rupture length (Figure 3), a 23% increase of L would be required to explain the observed 40% increase in aftershock occurrences. The similarity of the two estimates for the increase in L (typically 20% from observation and 23% from productivity scaling) suggests that the spatial spreading and the vigorous triggering characteristic of population A aftershock sequences are two related aspects of one common, single process, that ensemble-averaged clustering models like ETAS fail to explain. Transient diffusing aseismic deformation/creep triggering foreshocks and extra aftershocks is one potential candidate.

6. Discussion and Conclusions

Earthquake dynamics exhibit strong variability, owing to the complexity of the rupture process itself and to the heterogeneous nature of the crust. Episodic creep can occur without triggering a large rupture [*Marsan et al.*, 2013; *Brodsky and Lay*, 2014]. Large ruptures can occur without detectable signs of prior creep [*Johnston et al.*, 2006]. Our analyses suggest that stronger aftershock productivity following foreshock activity could reveal the occurrence of an aseismic deformation transient affecting both the preseismic and the postseismic phases, so that the sequence is equivalent to a compound rupture. However, this mechanism cannot be simply observed for individual sequences on the basis of seismicity data alone: natural variability in the earthquake numbers is large (Figure 3), so that the relationship only emerges when averaging over many sequences. Individual instances of compound ruptures that include a very slow initiation phase have been evidenced for several oceanic ridges or transform earthquakes [*Ihmlé and Jordan*, 1994; *McGuire et al.*, 2005]. Our observation differs from these for three reasons: oceanic earthquakes have relatively few aftershocks (cf. supporting information, section "Dependence on location"), possibly owing to high thermal gradients; the relationship between preseismic and postseismic enhanced activities is found on ensemble average, not for individual sequences; all tectonic contexts appear to be affected by this correlation. Despite the averaged character of these observations, they strengthen the possibility of better constraining the a priori probability of large ruptures by eventually tracking potential instances of slow deformation transients [*Brodsky and Lay*, 2014].

Acknowledgments
This work benefited from funding by the French ANR JC ASEISMIC project and by the EC FP7 REAKT project. Earthquake data were downloaded from quake.geo.berkeley.edu/anss.

The Editor thanks two anonymous reviewers for their assistance in evaluating this paper.

References

Ando, R., and K. Imanishi (2011), Possibility of Mw 9.0 mainshock triggered by diffusional propagation of after-slip from Mw 7.3 foreshock, *Earth Plan. Space*, *63*(7), 767–771.

Bouchon, M., H. Karabulut, M. Aktar, S. Ozalaybey, J. Schmittbuhl, and M. P. Bouin (2011), Extended nucleation of the 1999 Mw 7.6 Izmit earthquake, *Science*, *331*(6019), 877–880.

Bouchon, M., V. Durand, D. Marsan, H. Karabulut, and J. Schmittbuhl (2013), The long precursory phase of most large interplate earthquakes, *Nat. Geosci.*, *6*(4), 299–302.

Brodsky, E. E., and T. Lay (2014), Recognizing foreshocks from the 1 April 2014 Chile earthquake, *Science*, *344*(6185), 700–702.

Dieterich, J. (1994), A constitutive law for rate of earthquake production and its application to earthquake clustering, *J. Geophys. Res.*, *99*(B2), 2601–2618, doi:10.1029/93JB02581.

Hardebeck, J. L., K. R. Felzer, and A. J. Michael (2008), Improved tests reveal that the accelerating moment release hypothesis is statistically insignificant, *J. Geophys. Res.*, *113*, B08310, doi:10.1029/2007JB005410.

Helmstetter, A., and D. Sornette (2003), Foreshocks explained by cascades of triggered seismicity, *J. Geophys. Res.*, *108*(B10), 2457, doi:10.1029/2003JB002409.

Ihmlé, P. F., and T. H. Jordan (1994), Teleseismic search for slow precursors to large earthquakes, *Science*, *266*, 1547–1551.

Johnston, M. J. S., R. D. Borcherdt, A. Linde, and M. T. Gladwin (2006), Continuous borehole strain and pore pressure in the near field of the 28 September 2004 M 6.0 Parkfield, California, earthquake: Implications for nucleation, fault response, earthquake prediction, and tremor, *Bull. Seismol. Soc. Am.*, *96*(4), S56–S72.

Kato, A., K. Obara, T. Igarashi, H. Tsuruoka, S. Nakagawa, and N. Hirata (2012), Propagation of slow slip leading up to the 2011 Mw 9.0 Tohoku-Oki, *Science*, *335*(6069), 705–708.

Marsan, D., T. Reverso, A. Helmstetter, and B. Enescu (2013), Slow slip and aseismic deformation episodes associated with the subducting Pacific plate offshore Japan, revealed by changes in seismicity, *J. Geophys. Res. Solid Earth*, *118*, 4900–4909, doi:10.1002/jgrb.50323.

McGuire, J. J., M. S. Boettcher, and T. H. Jordan (2005), Foreshock sequences and short-term earthquake predictability on East Pacific Rise transform faults, *Nature*, *434*, 457–461.

Mignan, A. (2014), The debate on the prognostic value of earthquake foreshocks: A meta-analysis, *Sci. Rep.*, *4*, 4099, doi:10.1038/srep04099.

Ogata, Y. (1988), Statistical models for earthquake occurrences and residual analysis for point-process, *J. Am. Stat. Assoc.*, *83*(401), 9–27.